Metrol. Meas. Syst., Vol. 28 (2021) No. 1, pp. 161–179
DOI: 10.24425/mms.2021.136000

PAN POLSKA AKADEMIA NAUK

METROLOGY AND MEASUREMENT SYSTEMS
Index 330930, ISSN 0860-8229
www.metrology.wat.edu.pl

M&MS

A FEEDBACK WEIGHTED FUSION ALGORITHM WITH DYNAMIC SENSOR BIAS CORRECTION FOR GYROSCOPE ARRAY

Ding Yuan[1)], Yongyuan Qin[1)], Xiaowei Shen[2)], Zongwei Wu[2)]

1) *School of Automation, Northwestern Polytechnical University, Xi'an 710129, China* (✉ *yuanding31@mail.nwpu.edu.cn*, +86 29 8474 3382, *y.qinyongyuan@nwpu.edu.cn*)
2) *Xi'an Research Institute of High Technology, Hongqing Town, Xi'an 710025, China* (*x.shenxw602@gmail.com*, *z.zongweiwu@yahoo.cn*)

Abstract

Low-cost Micro-Electromechanical System (MEMS) gyroscopes are known to have a smaller size, lower weight, and less power consumption than their more technologically advanced counterparts. However, current low-grade MEMS gyroscopes have poor performance and cannot compete with quality sensors in high accuracy navigational and guidance applications. The main focus of this paper is to investigate performance improvements by fusing multiple homogeneous MEMS gyroscopes. These gyros are transformed into a virtual gyro using a feedback weighted fusion algorithm with dynamic sensor bias correction. The gyroscope array combines eight homogeneous gyroscope units on each axis and divides them into two layers of differential configuration. The algorithm uses the gyroscope array estimation value to remove the gyroscope bias and then correct the gyroscope array measurement value. Then the gyroscope variance is recalculated in real time according to the revised measurement value and the weighted coefficients and state estimation of each gyroscope are deduced according to the least square principle. The simulations and experiments showed that the proposed algorithm could further reduce the drift and improve the overall accuracy beyond the performance limitations of individual gyroscopes. The maximum cumulative angle error was −2.09 degrees after 2000 seconds in the static test, and the standard deviation (STD) of the output fusion value of the proposed algorithm was 0.006 degrees/s in the dynamic test, which was only 1.7% of the STD value of an individual gyroscope.

Keywords: inertial sensor, gyroscope array, weighted fusion, bias correction.

1. Introduction

Gyroscopes are applied in such diverse fields as vehicle navigation, autonomous vehicles, platform stabilization, and so on [1, 2]. Accurate estimates can be achieved over more extended periods by integrating high-quality gyroscopes and good initial estimates of the attitude. However, high-quality gyroscopes such as mechanical, fibre-optic, or ring laser sensors are too expensive

Article history: received June 20, 2020; revised November 14, 2020; accepted December 3, 2020; available online December 14, 2021.

for many applications and access to such sensors can be limited [3]. In recent years, *Micro-Electromechanical System* (MEMS) gyroscopes have been widely used with the advantages of small size, light weight, and low power consumption [4, 5]. However, the drift of MEMS gyroscopes is relatively high and the attitude estimation error accumulates quickly with time integration resulting in insufficient accuracy for attitude estimation or other applications requiring higher precision.

Generally, MEMS gyroscopes suffer from various types of errors that are broadly classified as deterministic errors and random errors [6, 7]. The deterministic errors that affect system performance are most commonly represented by bias, scale factor, and nonorthogonality. A considerable amount of literature has been contributed to the calibration of deterministic errors [8–11]. These errors can be removed by calibration, *i.e.* comparing the measured value to a known standard reference. However, this does not work in practice because the bias of a MEMS gyroscope changes significantly every time the device is powered up [12].

Sensor fusion using two or more different sensors has been carried out to overcome this problem. One solution is to utilise gravity and magnetic reference sensors for tilt and pan angle measurements respectively [13]. Accelerometers measure the Earth's gravitational vector, and magnetometers provide values for the magnetic field of the Earth which aids sensors with correcting the drift of the gyroscope. Traditionally, fusion algorithms such as the *extended Kalman filter* (EKF) and the *complementary filter* (CF) have been widely used [14, 15]. They can improve the estimation accuracy and lower the precision requirements of inertial sensors by fusing the complementary information of various heterogeneous sensors. However, those aiding sensors themselves suffer from performance degradation in some conditions [16–18]. Also, there is no redundancy in the method described above, as when one sensor fails it may affect the whole system. Achieving robustness and reliability in the performance of these angular rate sensors remains a significant challenge.

One idea is to make up an array of the same type of MEMS gyroscopes on the same sensitive axis and improve the accuracy aa well as reliability by utilising technology redundancy [19–21]. Its principle is that several homogeneous low-precision gyroscopes are combined to form an array and measure the same angular rate. David S. Bayard of the Jet Propulsion Laboratory first proposed the "virtual gyroscope" technology so that an optimal rate estimate could be obtained through an optimal filter fusing these measurements. The key to combining multiple gyroscopes for accuracy improvement lies in rate signal modelling and the *Kalman filter* (KF) design [22]. The results in [22] showed that the proposed "virtual gyroscope" could significantly reduce noise and bias instability as well as improve the overall accuracy beyond the performance limitations of individual gyroscopes. Subsequently, Chang Honglong of the Northwest Polytechnic University and others carried out similar research [23–27]. However, the methods above required these correlations to be estimated from sensor data. Also they were not able to estimate the correlations between the drift components of individual sensors. Furthermore, the dimension of the KF will increase with the numbers of sensors in the array which can lead to a formidable computational burden. On the other hand, the real rate signal is usually modelled directly as a specific random process driven by white noise. Unfortunately, it is difficult to choose an appropriate value for variance of white noise which is usually set empirically without any criteria. In recent years, a weighted averaging fusion algorithm has been regarded as a promising method for accuracy improvement of MEMS gyroscope arrays. Compared with existing algorithms, the weighted averaging fusion algorithm is simple and easy to implement. It has the advantages of optimality, unbiasedness and minimum mean square error. The weighted coefficient in the weighted fusion method reflects the confidence level of the sensor signal. Whether the weighted coefficient is reasonable or not is the key to determine the fusion performance. M. Tanenhaus

Metrol. Meas. Syst., Vol. 28 (2021), No. 1, pp. 161–179
DOI: 10.24425/mms.2021.136000

of Tanenhaus & Associates, Inc. has achieved high performance using eight gyroscopes per axis and optimal algorithms to minimise noise and drift [28]. The weights were determined by employing *principal component analysis* (PCA) to long records of array data which were optimal in the minimum mean-square sense. J. V. Richard presents an algorithm for obtaining the Allan covariance statistical model for an array of gyroscopes, including cross-correlations of individual random drift components [29]. The optimal weights were derived with the *Rate Random Walk* (RRW) matrix, and a weighted sum of the gyroscope signals using a fixed linear combination was given. With a 28-gyroscope array, results showed that the proposed virtual gyroscope had a drift spectral density 40 times smaller than that obtained by taking the average of individual gyroscope signals. However, in both cases, the fixed weights were derived from long records of calibration data that were obtained while the array was motionless. The fixed allocation of weights could not achieve the optimal state in a dynamic environment due to the consideration of environmental interference and other factors. Thus, it is crucial to estimate the weighted coefficient in real time.

To overcome the shortcomings of prior work, an array with multiple gyroscopes per axis was constructed, and a feedback weighted fusion algorithm was proposed for the gyroscope array. A model for the bias of gyroscopes was presented in which the estimation value of the gyroscope array at the previous moment was feedback into each gyroscope measurement. Then, the gyroscope variances were calculated recursively after correcting gyroscope bias which was inversely proportional to the weight factors under the criterion of minimum mean square error. Lastly, the weight factors of the gyroscope array were updated in each iteration, and an optimal estimation was obtained by taking a linear combination of individual gyroscope outputs.

The rest of this paper is organised as follows: Section 2 gives a brief description of the hardware used in the gyroscope array. In Section 3, a feedback weighted fusion algorithm is presented together with the weight factors of the gyroscope array updated in each iteration. In Section 4 and Section 5, the simulations and experiments are presented to demonstrate in detail how the procedures were implemented and to verify the validity of the proposed approach. Finally, Section 6 provides a brief conclusion.

2. MEMS gyroscope array design

In order to improve the signal quality of the MEMS gyroscope, redundant detection clusters are used in which the gyroscope is arranged linearly along each detection axis. Each gyroscope in the cluster operates independently and measures the angular rate around the tri-axis, as illustrated in Fig. 1a. The underlying rule for the gyro-board design is to mount the gyroscopes as close as possible for the convenience of using identical control and sampling circuitry. The circuit board serves as a rigid framework for the sensors as well as a means of control of the sensory output. As described in Fig. 1b, the sensor orientation is also given special consideration. To measure the same rotational rate, the input axis of all the units must be parallel. The eight MEMS units in each axis effectively form a gyroscope cluster with a minimum of separation between the sensors. The sensors are divided into two layers, with four sensors in each layer, and the direction of the sensing axis between layers is opposite. Within each layer, the sensors are arranged in pairs, and the driving axis and measuring axis of each pair of sensors are opposite to reduce the G sensitivity error caused by external force.

A diagram of the gyroscope array block setup (Fig. 2a) and a picture of the hardware implementation (Fig. 2b) are shown in Fig. 2. As shown in Fig. 2a, a *Field-Programmable Gate Array* (FPGA) and an ARM microcontroller are used in the hardware design. They communicate

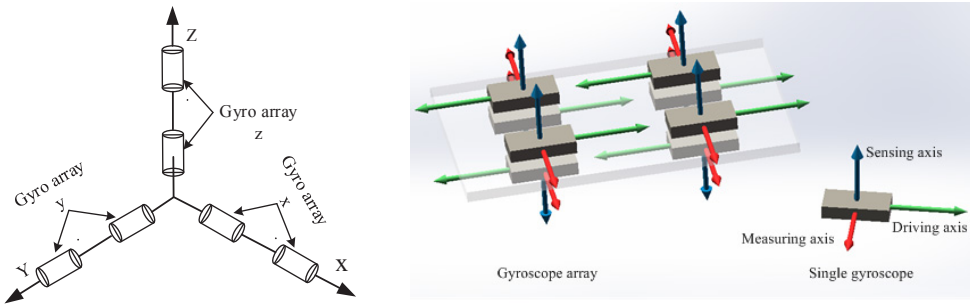

(a) Linear disposition of the gyroscope array. (b) One-axis configuration of the gyroscope array.

Fig. 1. Configuration of the gyroscope array.

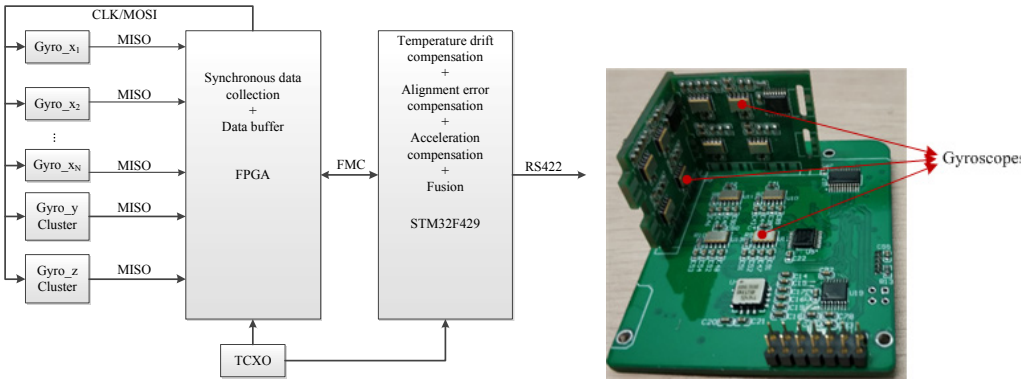

(a) Diagram of the gyroscope array. (b) Hardware of the gyroscope array.

Fig. 2. An implementation of the gyroscope array.

with each other through a *Flexible Memory Controller* (FMC) which provides high-speed data communication capabilities. A Temperature Compensated Xtal (crystal) Oscillator (TCXO) is used to provide a stable and reliable clock. All the gyroscopes are interfaced with the FPGA through a *Serial Peripheral Interface* (SPI) which includes a *Master Input Slave Output* (MISO) pin, *Master Output Slave Input* (MOSI) pin, and Clock (CLK) pin. The FPGA obtains data from rate registers and temperature registers in the gyroscopes, then saves the data in the buffers of the FPGA which works as an external *Static Random-Access Memory* (SRAM) of the ARM through the FMC. Furthermore, temperature compensation, calibration processing, fault tolerance mechanism and fusion filtering are implemented in the ARM. For each cluster, the measured data are subsequently fused to provide a better-measured signal for the angular rate of respective axis. Simultaneously, this structure provides the advantage of having a redundant inertial navigator in terms of the detection unit components, *i.e.* when one or more sensors in a detection cluster break down, they are removed from the calculation process while the system remains operational. The gyro array hardware, as shown in Fig. 2b, is composed of a mother board with a gyro array unit and two gyro array unit mounted daughter boards, and the three are installed orthogonally.

Metrol. Meas. Syst., Vol. 28 (2021), No. 1, pp. 161–179
DOI: 10.24425/mms.2021.136000

3. Feedback weighted fusion algorithm

To achieve the optimal estimation of the gyroscope array, a data fusion method using a feedback weighted fusion algorithm is proposed to obtain a linear combination of individual gyroscope output.

3.1. Mathematical model for the gyroscope array

For the purpose of combining the measurements of the gyros, it is critical to analyze and establish a reasonable model of output of a single MEMS gyro, as random noises corrupt it. Numerous experiments have shown that bias and zero-mean white noise, manifested as *Rate Random Walk* (RRW) and *Angle Random Walk* (ARW) noise are the dominant errors for low-grade MEMS gyroscopes after temperature drift compensation. RRW is the creep of angular velocity measurement of the output of the gyroscope, and ARW is the noise of the gyroscope output which will cause the creep of the angle when the ARW noise is integrated. Consequently, in the present study, the gyroscope can be modelled by:

$$\begin{cases} z_g = \omega + b + e \\ \dot{b} = v \end{cases}, \tag{1}$$

where z_g is the gyroscope output, ω is the real rate, b is a slowly changing bias driven by the RRW v, and e is the ARW white noise.

Each gyro measures the same angular rate in the N tri-axial gyroscope cluster, therefore (1) can be written as:

$$\begin{cases} z_{gi} = \omega + b_i + e_i \\ \dot{b}_i = v_i \end{cases} \quad i = 1, \ldots, N, \tag{2}$$

where z_{gi} is the output of the i^{th} gyroscope, ω is the real rate, e_i is the continuous-time white noise process denoted as ARW noise, and b_i is the slowly changing bias driven by the continuous-time white noise v_i, which represents the RRW noise.

The above quantities associated with one axis for the collection of N gyros are stacked into the following vectors. The same formulae are applied to the other two axes as well.

$$\boldsymbol{Z}_g = \omega + \boldsymbol{b} + \boldsymbol{e} \tag{3}$$

with $\boldsymbol{Z}_g = \begin{bmatrix} z_1 & z_2 & \cdots & z_N \end{bmatrix}^{\mathrm{T}}$, $\boldsymbol{b} = \begin{bmatrix} b_1 & b_2 & \cdots & b_N \end{bmatrix}^{\mathrm{T}}$, $\boldsymbol{e} = \begin{bmatrix} e_1 & e_2 & \cdots & e_N \end{bmatrix}^{\mathrm{T}}$.

3.2. Optimal weighted fusion algorithm

Over a long period, the RRW and ARW noises are both zero mean, but in a certain time window, usually from a few seconds to a few minutes, RRW creeps slowly. Thus, the RRW noise, manifested as a bias of gyroscopes, should be removed before weighted fusion. In this section, a straightforward predictor will be introduced, based on moving averages for practical implementation.

$$\begin{cases} b_i(k) = \dfrac{k-1}{k} b_i(k-1) + \dfrac{1}{k}\left(z_i(k) - \hat{\omega}(k-1)\right) \\ b_i(0) = 0 \end{cases}, \tag{4}$$

where $b_i(k)$ is the estimation of bias of the i^{th} gyroscope at time k, $b_i(0) = 0$, $z_i(k)$ is the measured signal of the i^{th} gyroscope at time k, and $\hat{\omega}(k-1)$ is the estimated rate of the gyroscope array using weighted fusion at time $k-1$.

The measurement noise can be regarded as white noise after removing the bias for the prior compensation of the measurements of the bias values. According to (3), it can be expressed as:

$$\boldsymbol{Y} = \mathbf{H}\,\omega + \boldsymbol{e}\,, \tag{5}$$

where ω is the real rate, $\boldsymbol{Y} = \begin{bmatrix} y_1 & y_2 & \cdots & y_N \end{bmatrix}^{\mathrm{T}}$ and is the output vector of gyroscopes after bias has been removed, and $\mathbf{H} = \begin{bmatrix} 1 & 1 & \cdots & 1 \end{bmatrix}^{\mathrm{T}}$ is the N-dimensional constant vector.

Consequently, multiple measurements of the gyroscope array are linearly combined. A virtual gyro signal can be obtained by taking a fixed linear combination of gyroscope signals. The weighted coefficient in the weighted fusion method reflects the confidence level of the sensor signal. Whether the weighted coefficient is reasonable or not is crucial in determining the fusion performance.

In some cases, the weights are derived from an independent static method which ignores the objectivity of multi-sensor systems in a dynamic environment. Moreover, the static allocation of weights does not reflect the real performance of the sensors. In general, the random errors of sensors obey normal distribution or approximately obey normal distribution, and the weighted coefficients are calculated with the variance of the measurement from each gyro. The variance of each sensor signal is influenced by measurement accuracy, transmission error, environmental noise, and disturbance and it does not stay unchanged in practice. The variance cannot be merely equivalent to the variance parameters of the sensor itself or specified by experience, therefore it must be estimated in real time.

The least square method is used to estimate the rate $\hat{\omega}$ of the gyroscope array. The criterion of the least square estimation is to minimise the sum of the squares of the errors:

$$\arg\min\left(Jw\left(\hat{\omega}\right)\right) = \arg\min\left(\boldsymbol{Y} - \mathbf{H}\,\hat{\omega}\right)^{\mathrm{T}} \boldsymbol{W}\left(\boldsymbol{Y} - \mathbf{H}\,\hat{\omega}\right), \tag{6}$$

where

$$\boldsymbol{W} = \begin{bmatrix} w_1 & & & \\ & w_2 & & \\ & & \cdots & \\ & & & w_n \end{bmatrix}$$

is a positive definite diagonal weighted matrix.

For the partial derivative:

$$\frac{\partial Jw\left(\hat{\omega}\right)}{\partial \hat{\omega}} = -\mathbf{H}^{\mathrm{T}}\left(\boldsymbol{W} + \boldsymbol{W}^{\mathrm{T}}\right)\left(\boldsymbol{Y} - \mathbf{H}\,\hat{\omega}\right) = 0. \tag{7}$$

The corresponding parameter estimators satisfy:

$$\hat{\omega} = \left(\mathbf{H}^{\mathrm{T}}\boldsymbol{W}\mathbf{H}\right)^{-1}\mathbf{H}^{\mathrm{T}}\boldsymbol{W}\,\boldsymbol{Y} = \sum_{i=1}^{N} w_i y_i\,, \tag{8}$$

where w_i is the weighted coefficient for the i^{th} gyroscope which satisfies $\sum_{i=1}^{N} w_i = 1$.

Metrol. Meas. Syst., Vol. 28 (2021), No. 1, pp. 161–179
DOI: 10.24425/mms.2021.136000

Suppose the mean and variance of the measurement noise satisfies:

$$\begin{cases} E[e_i] = 0 \\ E\left[e_i^2\right] = \sigma_i^2 \end{cases}, \quad i = 1, 2, \ldots, N, \tag{9}$$

where σ_i^2 is the variance of the i^{th} gyroscope and represents the accuracy of the sensor. Moreover, the sensor accuracy is higher with a smaller variance. According to the optimal weighted theory [30], the weights are satisfied:

$$w_i = \frac{\dfrac{1}{\sigma_i^2}}{\sum\limits_{j=1}^{N} \sigma_j^2}. \tag{10}$$

It is clear that under the criterion of the minimum mean square error, the weighted coefficient is inversely proportional to the measurement variance of the sensor. Thus, the weighted coefficient can be transformed into estimation of measurement variance of the sensor.

Gyroscope variance is the result of its precision, measurement error, and environmental interference, it is not unchanged in practical engineering. Thus, it cannot be simply equated with the sensor variance parameters or specified by experience. The variance needs to be estimated in real time by an algorithm. In this case, the variances of the sensors are calculated at each time step.

Step 1: Calculate the mean of the gyroscope array at a given time. If $y_i(k)$ is the k^{th} measure from the i^{th} gyroscope, then the mean of the gyroscope array can be calculated as follows:

$$\bar{y}(k) = \frac{1}{N} \sum_{i=1}^{N} y_i(k). \tag{11}$$

Step 2: Estimate the variance of the gyroscopes. For the i^{th} gyroscope, the variance of the gyroscope is given using an average of M consecutive samples:

$$\begin{aligned} \hat{\sigma}_i^2(k) &= E\left[(y_i(k) - \bar{y}(k))^2\right] \\ &= \frac{1}{M} \sum_{j=0}^{M-1} (y_i(k-j) - \bar{y}(k-j))^2. \end{aligned} \tag{12}$$

Then the variance estimator is written as a recursive form:

$$\begin{cases} \sigma_i^2(k) = \dfrac{k-1}{k} \sigma_i^2(k-1) + \dfrac{1}{k} \hat{\sigma}_i^2(k) \\ \sigma_i^2(0) = 0 \end{cases}. \tag{13}$$

In this way, the algorithm has an adaptive character, the data frame used to estimate new measurements updates the variance of the gyro signals and the weights associated with each sensor are re-estimated at each measurement step.

The block diagram of the algorithm is shown in Fig. 3. The algorithm consists of a bias correction block and an optimal weight fusion block. And the detailed steps of the proposed method are shown below.

Algorithm

Input: the output vector of the gyroscope array, $Z = [z_1, z_2 \quad \cdots \quad z_N]^{\mathrm{T}}$;

Output: the estimated rate of the gyroscope array, $\hat{\omega}$;

Step 1: Initialise the gyroscope bias and the variance;

Step 2: Estimate the bias b_i of the gyroscopes using (4);

Step 3: Compensate the original measurements with the bias estimates using (3);

Step 4: Calculate of the gyroscope variance σ_i^2 using (13);

Step 5: Compute the weight factors w_i using (10);

Step 6: Estimate the rate $\hat{\omega}$ by taking a linear combination of individual gyroscope outputs using (8);

Step 7: Return to Step 2.

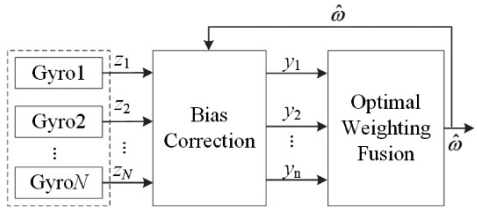

Fig. 3. Block diagram of the algorithm.

4. Simulation results

Numerical simulations of an array of six gyros were performed to test the validity of the proposed method. The output signals of the gyroscope array were simulated by the gyroscope model in (1), and the data rate of the sensors was chosen as 50 Hz. Gyro bias was considered as constant to show the efficiency of the proposed method. The bias quality of individual gyros is shown in Table 1, where the ARW and RRW noises for the gyroscopes were assumed to be $1\times10^{-6}\,^{\circ}/\sqrt{\mathrm{s}}$ and $1\times10^{-3}\,^{\circ}/\sqrt{\mathrm{s}^3}$ respectively. The Simulink model is shown in Fig. 4. Additionally, results for the static and dynamic simulations are also presented.

Table 1. Bias of individual gyros.

Gyro	1	2	3	4	5	6
Bias Stability degree/s	0.1	–0.1	0.2	–0.2	0.3	–0.05

Standard deviation (STD, 1σ) of the rate errors was adopted to quantify the measurement precision of the rate signal in the condition. The mathematical expression of the STD is defined as:

$$\sigma = \sqrt{\frac{1}{n-1}\sum_{k=1}^{n}(\hat{\omega}_k - \omega_k)^2}, \tag{14}$$

where ω_k is the real rate signal of the k^{th} time, $\hat{\omega}_k$ is the estimation of ω_k and n is the length number of rate samples.

Metrol. Meas. Syst., Vol. 28 (2021), No. 1, pp. 161–179
DOI: 10.24425/mms.2021.136000

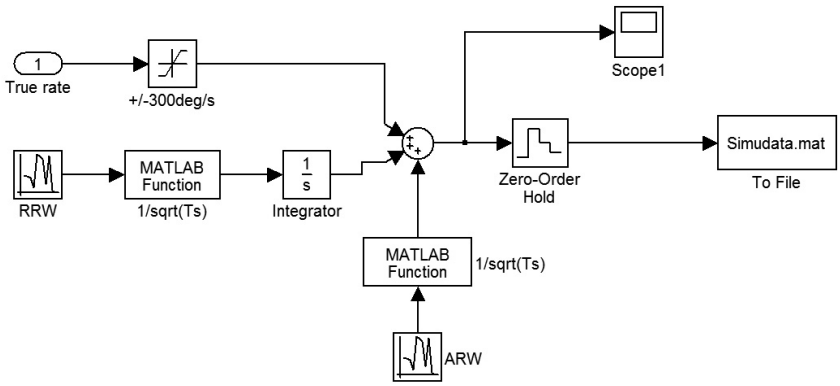

Fig. 4. The Simulink model for generating outputs of the gyroscope array signals.

4.1. Static simulations

For the static simulation, the input rate in the Simulink model was set to $\omega = 0$ to evaluate the performance. The output signals of the gyroscope array generated by the Simulink model are shown in Fig. 5. Based on the values in Table 1, 2000 seconds of gyroscope data were simulated. Figure 5 shows the simulation results of individual gyroscopes and the fusion result. The original outputs of individual gyroscopes with different gyro biases are shown in Fig. 5a. A significant reduction of the noise level can be easily observed from Fig. 5b when it performs the fusion algorithm.

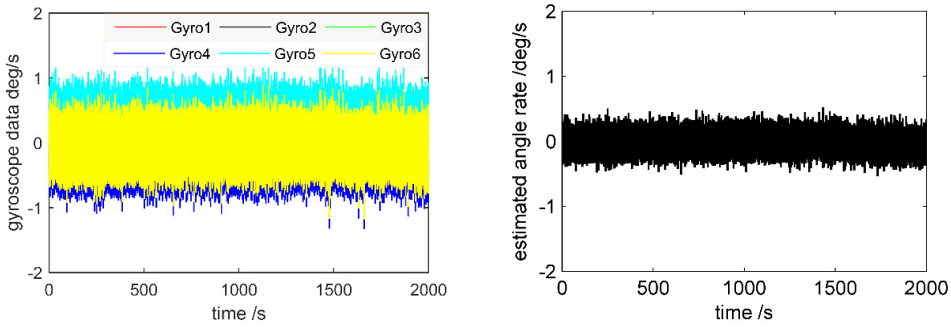

(a) Original outputs of individual gyroscopes.

(b) Estimated rate of the gyroscope array.

Fig. 5. Static simulation of the gyroscope array.

Figure 6 presents a comparison of integration angle errors between the original output of individual gyroscopes and the estimations using different algorithms. Figure 6a shows that the integration angle derived from each gyro suffers from long-term accumulated errors caused by gyro biases. Gyroscope5 had the most significant angle error, reaching 577.3 degrees after 2000 seconds. Furthermore, Gyro 6 had the smallest angle error with a cumulative error of 122.6 degrees in 2000 seconds. The cumulative error of individual gyroscopes is consistent with the definition in Table 1. The larger the bias is, the larger the cumulative error. Thus, it is necessary to fuse the gyro array to obtain a more accurate output.

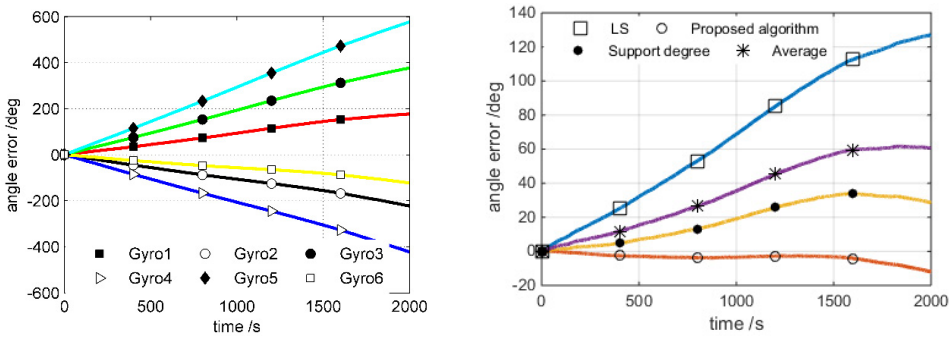

(a) Angle errors of individual gyroscopes.

(b) Angle errors using different algorithms.

Fig. 6. Integration angle error before and after fusion.

Figure 6b presents a comparison of the angle errors using different fusion algorithms such as the *least square* (LS) method [31], support degree function (where the weighting factors are acquired by calculating the supporting degree matrix among multi-sensor observations to obtain observational fusion values) [32], averaging methods, and the proposed feedback weighted fusion algorithm. The results of the 1σ error are illustrated in Table 2. These algorithms provided relatively good results compared with pre-fusion. Among them, the LS method had significant angle errors due to the impact of bias. On the contrary, the proposed feedback weighted fusion algorithm worked best. Table 2 displays the maximum error (Max) and STD for the different estimation methods in Fig. 6. It is worth noting that the maximum cumulative angle errors of the proposed algorithm are 11.98 degrees in 2000 seconds, while it is 127.1 degrees using the LS method. Compared to the error in the smallest drift gyro, *i.e.* gyro 6, the angle error after utilising the fusion algorithm was 9.8%. It shows that the output accuracy of the gyro array was much improved after fusion, especially when using the proposed feedback weighted fusion.

Table 2. Error result comparison.

Error before fusion			**Error after fusion**	
Gyro number	**Max (degrees)**	**Algorithm**	**Max (degrees)**	**STD (degree/s)**
1	177.4	Proposed algorithm	12.0	0.0604
2	222.6	LS	127.1	0.1217
3	377.4	Support degree	28.7	0.1408
4	422.6	Average	60.7	0.1187
5	577.4			
6	122.6			

The estimated bias and weight of individual gyroscopes using the proposed feedback weighted fusion algorithm are shown in Fig. 7. It can be seen that the estimated bias was consistent with the definition in Fig. 7a and Table 1. The result shows that the proposed algorithm could estimate and correct gyro bias effectively. In Fig. 7b, the weights of the individual gyroscopes are presented. As was expected, if the bias of the gyro was small, then the weight was relatively high, and the fusion could rely more on the corresponding gyro output. Conversely, if the bias of the gyro was significant, then the weight was relatively small.

Metrol. Meas. Syst., Vol. 28 (2021), No. 1, pp. 161–179
DOI: 10.24425/mms.2021.136000

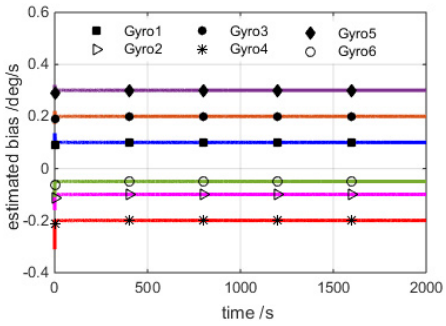

(a) Estimated bias of individual gyroscopes.

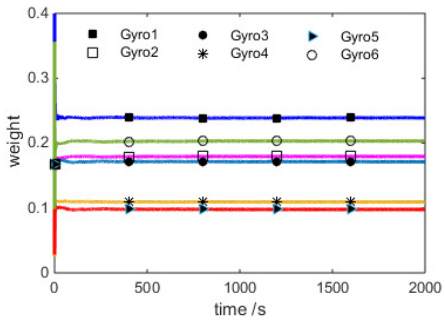

(b) Weight of individual gyroscopes.

Fig. 7. Parameter estimation of the gyroscope arrays in the static simulation.

4.2. Sinusoidal rate simulation

As for the sinusoidal rate simulation, the input rate signal was given by a sinusoidal signal as $\omega = 20 \times \sin(\pi t/200)$ degrees/s with frequency $f = 2.5 \times 10^{-3}$ Hz and phase $\varphi_0 = 0$. The Simulink model generated the output signals of the gyroscope array. The simulation results of individual gyroscopes and the fusion result are illustrated in Fig. 8. The original outputs of individual gyroscopes with different gyro biases are shown in Fig. 8a. Figure 8b shows the estimated rate of the gyroscope array using the proposed feedback weighted fusion algorithm. Data denoted as "Ref" and "Estimated" are reference rates and estimated rates respectively. It can be seen that the proposed algorithm can filter the drift of the gyro and provide good angle rate estimation in dynamic conditions.

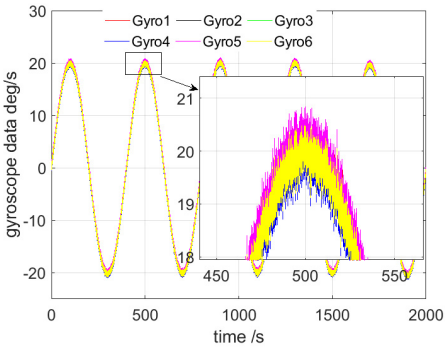

(a) Original outputs of the individual gyroscopes.

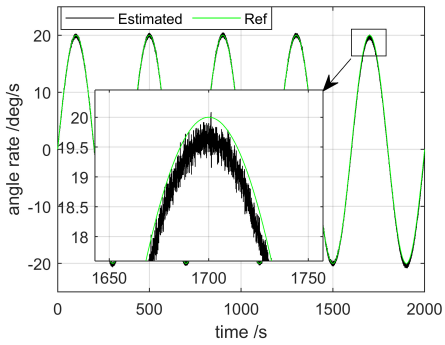

(b) Estimated rate of the gyroscope array.

Fig. 8. Sinusoidal rate simulation of the gyroscope array.

A comparison of estimated errors using different fusion algorithms is shown in Fig. 9. The estimated bias and weight of the individual gyroscopes using the proposed feedback weighted fusion algorithm are shown in Fig. 10a and Fig. 10b respectively.

The compared results are illustrated in Table 3. The results show that these algorithms can significantly improve performance under dynamic conditions. However, compared with the existing algorithms, it is more effective to use the proposed feedback weighted method to fuse the

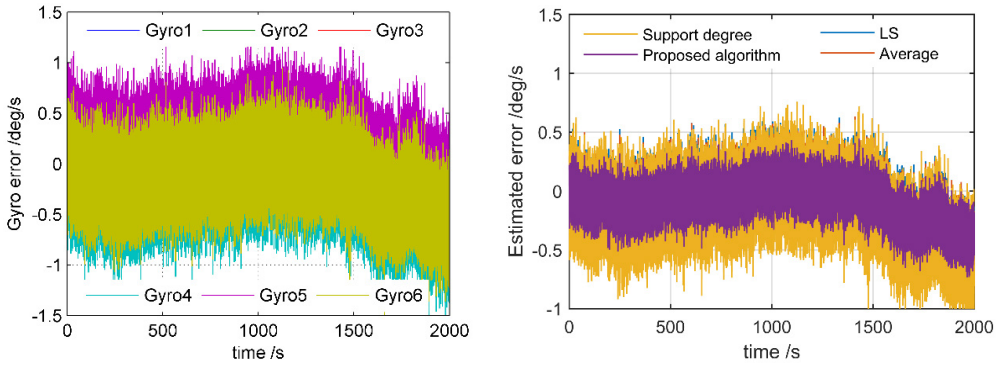

(a) Output errors of individual gyroscopes.

(b) Estimated errors using different algorithms.

Fig. 9. Error comparison before and after fusion.

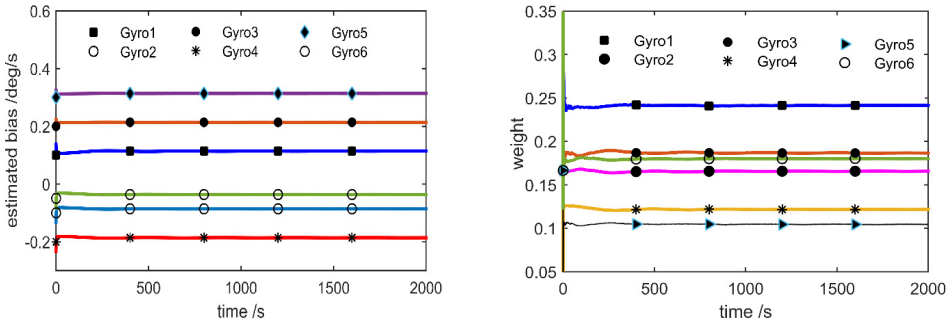

(a) Estimated bias of individual gyroscopes.

(b) Weights of individual gyroscopes.

Fig. 10. Parameter estimation of the gyroscope array in the dynamic simulation.

gyroscopes. This can be explained as follows: the algorithm uses the gyroscope array estimation value to recur the gyroscope bias and then corrects the gyroscope array measurement value. Based on this feedback information, optimum weighted fusion is obtained. Table 3 reveals that

Table 3. Error result comparison for different algorithms.

Error before fusion				**Error after fusion**	
Gyro number	**Mean (degree/s)**	**STD (degree/s)**	**Algorithm**	**Mean (degree/s)**	**STD (degree/s)**
1	–0.01	0.27	Proposed algorithm	–0.09	0.15
2	–0.21	0.27	LS	–0.02	0.20
3	0.09	0.27	Support degree	–0.16	0.24
4	–0.31	0.27	Average	–0.06	0.21
5	0.19	0.27			
6	–0.16	0.27			

Metrol. Meas. Syst., Vol. 28 (2021), No. 1, pp. 161–179
DOI: 10.24425/mms.2021.136000

both the mean and STD of the estimated error were reduced by fusing multiple measurements from the gyroscope array. Compared with Gyro 5, the STD of the estimated error of the proposed algorithm resulted in a 55.5% reduction.

5. Experiment comparison

The signals of the gyroscope array were transmitted to a computer running the proposed fusion method in real time to test the validity of both the system and the proposed method. Figure 11 shows the setup of the experiment. The sampling frequency was 50 Hz when the static test and the dynamic test were implemented. The x-axis signals of all eight gyroscopes were analysed here.

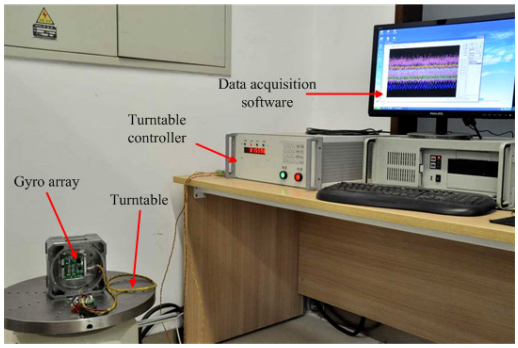

Fig. 11. Setup of the experiment.

5.1. Static test

The static rate signals of the gyroscopes were collected statically on a table for 2000 seconds. The proposed algorithm was compared with the support degree algorithm, least square algorithm, and a mean filter which averaged the outputs of individual gyroscopes. The original rate signals of individual gyroscopes and the processed with different methods are given in Fig. 12. In Fig. 12b,

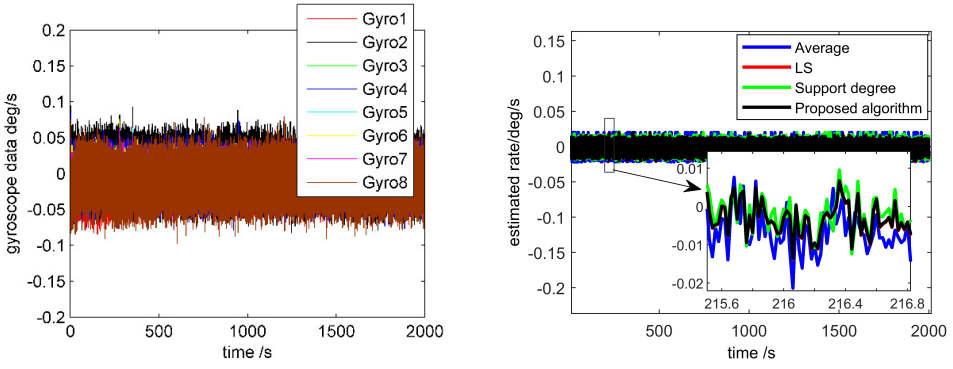

(a) Outputs of the individual gyroscopes.

(b) Estimated rates of the gyroscope array.

Fig. 12. Results of the static test.

the drift is reduced significantly by these algorithms. Table 4 presents the Mean and the STD of the outputs to demonstrate the effectiveness of those methods. Compared with Gyro 3, the 1σ errors were reduced from 0.011 degree/s to 0.004 degree/s.

Table 4. Result comparison for the static test.

Error before fusion				**Error after fusion**	
Gyro number	**Mean (degree/s)**	**STD (degree/s)**	**Algorithm**	**Mean (degree/s)**	**STD (degree/s)**
1	–0.017	0.017	Proposed algorithm	–0.002	0.004
2	0.001	0.026	LS	–0.003	0.005
3	–0.005	0.011	Support degree	–0.002	0.006
4	–0.006	0.018	Average	–0.004	0.006
5	–0.002	0.011			
6	–0.001	0.013			
7	0.004	0.011			
8	–0.010	0.021			

In Fig. 13, the angular rates are integrated to reflect the angle error obtained from the gyros. Figure 13a) shows that the integration angles derived from the gyros varied widely. For example, Gyro 1 had the most significant angle error, reaching 33.2 degrees in 2000 seconds, while the cumulative error of Gyro 6 was only –0.82 degree. A comparison of the angle errors using different fusion algorithms is presented in Fig. 13b. It can be seen that these algorithms provide reasonably good results compared with pre-fusion. Among them, the maximum cumulative angle error using the proposed algorithm is –2.09 degrees in 2000 seconds. The corresponding errors for the simple average, the support algorithm and the least square algorithm are 8.85 degrees, 3.96 degrees, and 5.36 degrees, respectively. It shows that the output accuracy of the gyro array is much improved after fusion, especially when using the proposed feedback weighted fusion algorithm.

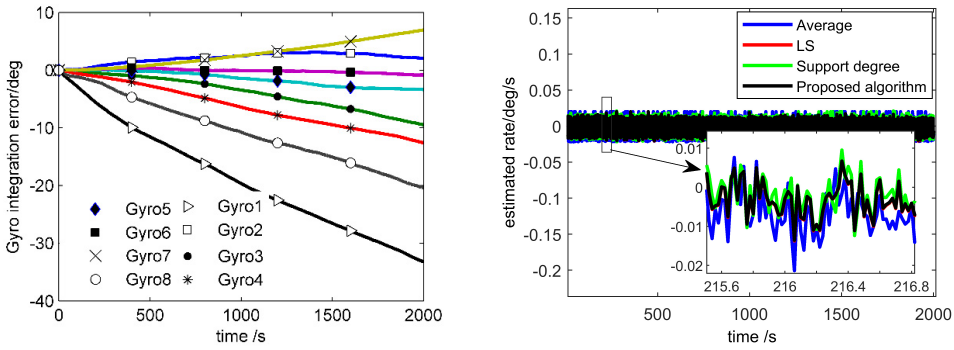

(a) Angle errors of individual gyroscopes.

(b) Angle errors using different algorithms.

Fig. 13. Integration angle error before and after fusion.

The estimated bias and weight of each gyroscope using the proposed feedback weighted fusion algorithm are shown in Fig. 14a and Fig. 14b. The weights are inversely proportional to the

Metrol. Meas. Syst., Vol. 28 (2021), No. 1, pp. 161–179
DOI: 10.24425/mms.2021.136000

measurement variance of the gyroscopes after removing the bias. The fusion weights are small when individual gyroscope errors are significant and these results are consistent with what was expected.

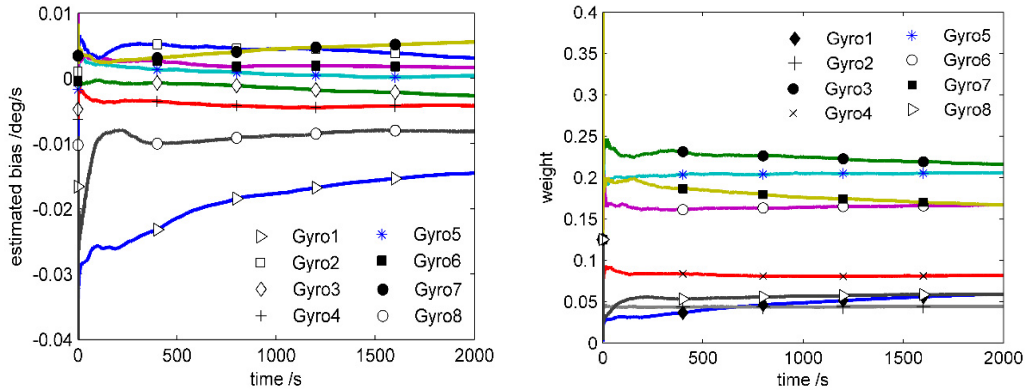

(a) Estimated bias of individual gyroscopes.

(b) Weight of individual gyroscopes.

Fig. 14. Parameter estimation of the gyroscope arrays in the static experiment.

5.2. Sinusoidal Rate Test

The turntable was set to rotate with the input rate signal $\omega = -25\times\cos(0.2\pi t + 0.3\pi)$ degrees/s in the dynamic test. The outputs of individual gyroscopes are shown in Fig. 15, while the fusion results and estimated errors are shown in Fig. 16. A comparison of the results is illustrated in Table 5. The results show that all these algorithms can improve performance significantly under dynamic conditions. Among them, the STD of the proposed algorithm is 0.006 degree/s, and the corresponding results of the simple average, the support algorithm, and the least square algorithm are 0.155 degree/s, 0.117 degree/s, and 0.009 degree/s, respectively. The STD of the proposed algorithm is only 1.7% of the value of Gyro 5.

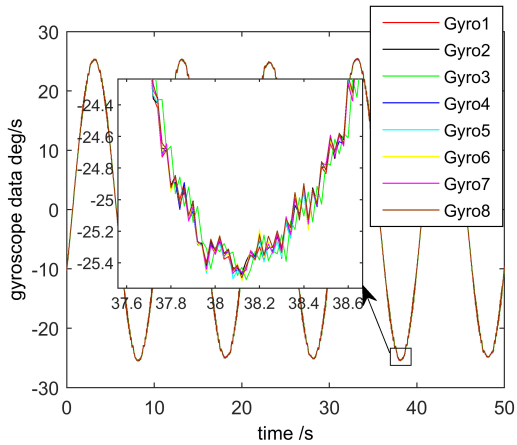

Fig. 15. Original output of individual gyroscopes.

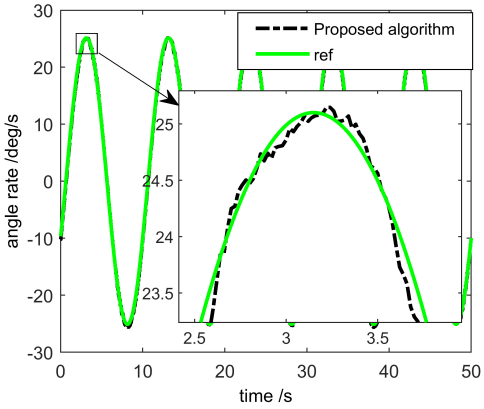

(a) Estimated rate of the gyroscope array.

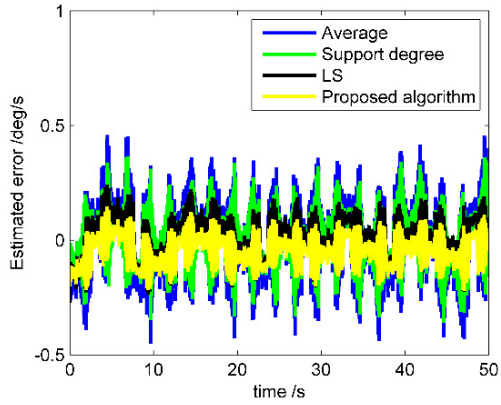

(b) Estimated errors.

Fig. 16. Sinusoidal rate fusion of the gyroscope array.

Table 5. Comparison of results for the dynamic test.

Gyro number	STD (degree/s)	Algorithm	STD (degree/s)
1	0.350	Proposed algorithm	0.006
2	0.350	LS	0.009
3	0.406	Support degree	0.117
4	0.351	Average	0.155
5	0.350		
6	0.351		
7	0.351		
8	0.351		

6. Discussion and conclusions

The performance of the feedback weighted fusion algorithm for gyroscope arrays was explored and analysed both in static and dynamic conditions. Simulations and experiments were carried out to quantify the accuracy of the combined rate signals. The simulation results indicate that the proposed algorithm can efficiently estimate and correct gyro bias. Moreover, the weighted coefficients and state estimation for each gyroscope recurred in real time according to the revised measurement value. The weights were inversely proportional to the measurement variance of the gyroscopes after removing the bias.

Eight MEMS gyroscopes per axis were utilised to develop a gyroscope array system. The experiments showed that the accuracy was much improved after fusion both in static and dynamic conditions. The maximum cumulative angle error was –2.09 degrees after 2000 seconds in the static test, and the STD of the proposed algorithm was 0.006 degree/s in the dynamic test which was only 1.7% of the value for an individual gyroscope.

Compared with existing algorithms, the feedback weighted fusion algorithm is simple and easy to implement. It has the advantages of optimality, unbiasedness, and minimum mean square

Metrol. Meas. Syst., Vol. 28 (2021), No. 1, pp. 161–179
DOI: 10.24425/mms.2021.136000

error. The optimal weights can be updated in each iteration and an optimal estimation is obtained by taking a linear combination of individual gyroscope outputs. The proposed algorithm resulted in a reduction of the combined gyro drift. Also performance improved significantly. This means that low-grade MEMS gyros can be used in much broader applications.

Author Contributions: Ding Yuan contributed to the design of the algorithms and the hardware. Yongyuan Qin also participated in the design of the algorithm. Xiaowei Shen designed the structure of the gyroscope array. Zongwei Wu developed the software used to collect the experimental data. All the authors of this article provided substantive comments.

Conflicts of Interest: The authors declare no conflict of interest.

References

[1] Wang, Y. L., Soltani, M., & Hussain, D. M. A. (2017). An attitude heading and reference system for marine satellite tracking antenna. *IEEE Transactions on Industrial Electronics*, *64*(4), 3095–3104. https://doi.org/10.1109/TIE.2016.2633529

[2] Hua, M. D., Ducard, G., Hamel, T., Mahony, R, & Rudin, K. (2014). Implementation of a nonlinear attitude estimator for aerial robotic vehicles. *IEEE Transactions on Control Systems Technology*, *22*(1), 201–213. https://doi.org/10.1109/TCST.2013.2251635

[3] Vittorio, M. N. P., Antonello, C., Lorenzo, V., Martino, D. C., & Carlo, E. C. (2017). Gyroscope technology and applications: a review in the industrial perspective. *Sensors*, *17*(10), 2284–2305. https://doi.org/10.3390/s17102284

[4] Shen, X. W., Yao, M. L., Jia, W. M., & Yuan, D. (2012). Adaptive complementary filter using fuzzy logic and simultaneous perturbation stochastic approximation algorithm. *Measurement*, *45*(5), 1257–1265. https://doi.org/10.1016/j.measurement.2012.01.011

[5] Ghasemi-Moghadam, S., & Homaeinezhad, M. R. (2018). Attitude determination by combining arrays of MEMS accelerometers, gyros, and magnetometers via quaternion-based complementary filter. *International Journal of Numerical Modelling: Electronic Networks, Devices and Fields*, *31*(3), 1–24. https://doi.org/10.1002/jnm.2282

[6] Shashi, P., Vipan, K., & Amod, K. (2017). A comprehensive overview of inertial sensor calibration techniques. *Journal of Dynamic Systems, Measurement, and Control*, *139*(1), 1–11. https://doi.org/10.1115/1.4034419

[7] El-Sheimy, N., Hou, H., & Niu, X. (2008). Analysis and modeling of inertial sensors using Allan variance. *IEEE Transactions on Instrumentation and Measurement*, *57*(1), 140–149. https://doi.org/10.1109/TIM.2007.908635

[8] Niu, X., Li, Y., Zhang, H., Wang, Q., & Ban, Y. (2013). Fast thermal calibration of low-grade inertial sensors and inertial measurement units. *Sensors*, *13*(9), 12192–12217. https://doi.org/10.3390/s130912192

[9] El-Diasty, M., & Pagiatakis, S. (2008). Calibration and stochastic modeling of inertial navigation sensor errors. *Journal of Global Positioning Systems*, *7*(2), 170–182. https://doi.org/10.5081/jgps.7.2.170

[10] Jixin, L., Ankit, A. R., Yukinori K., & Takanori E. (2016). A method of low-cost IMU calibration and alignment. *Proceedings of the 2016 IEEE/SICE International Symposium on System Integration*, Japan. https://doi.org/10.1109/SII.2016.7844027

[11] Fang, B., Chou, W. S., & Ding, L. (2014). An optimal calibration method for a MEMS inertial measurement unit. *International Journal of Advanced Robotic Systems*, *11*, 1–14. https://doi.org/10.5772/57516

[12] Jean-Philippe, D., Henrik, M., & Dan R. (2006). Bias aware Kalman filters: comparison and improvements. *Advances in Water Resources. 29*(5), 707–718. https://doi.org/10.1016/j.advwatres.2005.07.006

[13] Gebre-Egziabher, D., Hayward, R. C., & Powell, J. D. (2004). Design of multi-sensor attitude determination systems. *IEEE Transactions on Aerospace and Electronic Systems*, *40*(2), 627–649. https://doi.org/10.1109/TAES.2004.1310010

[14] Shen, X., Yuan, D., Chang, R., & Jin, W. (2019). A nonlinear observer for attitude estimation of vehicle-mounted satcom-on-the-move. https://doi.org/10.1109/JSEN.2019.2918381 *IEEE Sensors Journal*, *19*(18), 8057–8066.

[15] Wu, Z. M., Sun, Z. G., Zhang, W. Z., & Chen, Q. (2016). A novel approach for attitude estimation based on MEMS inertial sensors using nonlinear complementary filters. *IEEE Sensors Journal*, *16*(10), 3856–3864. https://doi.org/10.1109/JSEN.2016.2532909

[16] Thisura, H., & Munasinghe, S. R. (2017). Accurate attitude estimation under high accelerations and magnetic disturbances. *Proceedings of MERCon*, Sri Lanka. https://doi.org/10.1109/MERCon.2017.7980452

[17] Maliňák, P., Soták, M., Kaňa, Z., Baránek, R., & Duník, J. (2018). Pure-inertial AHRS with adaptive elimination of non-gravitational vehicle acceleration. *Proceedings of IEEE/ION Position, Location and Navigation Symposium (PLANS)*, USA. https://doi.org/10.1109/PLANS.2018.8373445

[18] Xing, L, Hang, Y. J., Xiong, Z., Liu, J. Y., & Wan, Z. (2016). Accurate attitude estimation using ARS under conditions of vehicle movement based on disturbance acceleration adaptive estimation and correction. *Sensors*, *16*(10), 1716–1731. https://doi.org/10.3390/s16101716

[19] Simon, K. K., & Luminita-Cristiana T. (2011). *Improving MEMS gyroscope performance using homogeneous sensor fusion* [Master's Thesis, Aalborg University, Denmark, May 2011]. https://projekter.aau.dk/projekter/files/52687369/11gr1033_ImprovingMEMS.pdf

[20] Yigiter, Y., & Naser, E. (2011). An optimal sensor fusion method for skew-redundant inertial measurement units. *Journal of Applied Geodesy*, *5*(2), 99–115. https://doi.org/10.1515/jag.2011.010

[21] John-Olof, N., & Isaac, S. (2016). Inertial sensor arrays – A literature review. *European Navigation Conference*, Finland. https://doi.org/10.1109/EURONAV.2016.7530551

[22] Bayard, D. S., & Ploen, S. R. (2003). High accuracy inertial sensors from inexpensive components. U.S. Patent No. 20030187623A1, 2 October 2003. https://patents.google.com/patent/US6882964B2/en

[23] Chang, H. L., Xue, L., Qin, W., Yuan, G. M., & Yuan, W. Z. (2008). An integrated MEMS gyroscope array with higher accuracy output. *Sensors*, *8*(4), 2886–2899. https://dx.doi.org/10.3390/s8042886

[24] Xue, L., Wang, L. X., Xiong, T., Jiang, C. Y., & Yuan, W. Z. (2014). Analysis of dynamic performance of a Kalman filter for combining multiple MEMS gyroscopes. *Micromachines*, *5*(4), 1034–1050. https://doi.org/10.3390/mi5041034

[25] Jiang, C., Xue, L., Chang, H., Yuan, G., & Yuan, W. (2012). Signal processing of MEMS gyroscope arrays to improve accuracy using a 1st order Markov for rate signal modeling. *Sensors*, *12*(2), 1720–1737. https://doi.org/10.3390/s120201720

[26] Yuan, G., Yuan, W., Xue L., Xie J., & Cha H. (2015). Dynamic performance comparison of two Kalman filters for rate signal direct modeling and differencing modeling for combining a MEMS gyroscope array to improve accuracy. *Sensors*, *15*(11), 27590–27610. https://dx.doi.org/10.3390/s151127590

[27] Ji, X. (2015). Research on signal processing of MEMS gyro array. *Mathematical Problems in Engineering*, *2015*, 120954, 1–6. https://doi.org/10.1155/2015/120954

[28] Tanenhaus, M. (2012). Miniature IMU/INS with optimally fused low drift MEMS gyro and accelerometers for applications in GPS-denied environments. *Proceedings of the 2012 IEEE/ION Position, Location and Navigation Symposium*, USA. https://doi.org/10.1109/PLANS.2012.6236890

Metrol. Meas. Syst., Vol. 28 (2021), No. 1, pp. 161–179
DOI: 10.24425/mms.2021.136000

[29] Richard, J. V., & Ahmed, S. Z. (2017). Reduced-drift virtual gyro from an array of low-cost gyros. *Sensors*, *17*(2), 352–369. https://doi.org/10.3390/s17020352

[30] Grigorie, T. L., & Botez R. M. (2013). A redundant aircraft attitude system based on miniaturized gyro clusters data fusion. *EuroCon 2013*, Croatia, 1992–1999. https://doi.org/10.1109/EUROCON.2013.6625253

[31] Ren, Y., Ge, Y., & Bai, X. (2012). Research on optimal weight choice of multi-MEMS gyroscope data fusion. *Applied Mechanics and Materials*, *192*, 351–355. https://doi.org/10.4028/www.scientific.net/AMM.192.351

[32] Zhang, W., Quan, L., & Zhang, K. (2012). Multi-layer track fusion algorithm based on supporting degree matrix. *Journal of Electronics (China)*, *29*, 229–237. https://doi.org/10.1007/s11767-012-0812-0

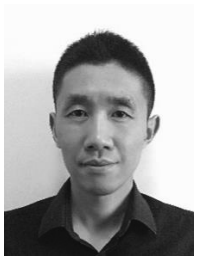

Ding Yuan received the B.S. and M.S. degree in electronic engineering from the Xi'an Research Institute of High Technology, Xi'an, China, in 2005 and 2012, respectively. His primary research interests are inertial sensors, integrated navigation and mobile satellite communication. He is currently working on his Ph.D. thesis in precision instrument and machinery at the School of Automation, Northwestern Polytechnical University, Xi'an, China.

Xiaowei Shen received his M.S. and Ph.D. degrees in information engineering from the Xi'an Research Institute of High Technology, Xi'an, China. He is currently a teacher with the Department of Electronic and Information Engineering, Xi'an Research Institute of High Technology. His research interests include array signal processing, attitude determination and mobile satellite communication.

Yongyuan Qin is currently a Professor and Doctoral Supervisor with the School of Automation, Northwestern Polytechnical University, Xi'an, China. His research interests include inertial navigation and integrated navigation.

Zongwei Wu received the M.S. and Ph.D. degree in electronic engineering from the Xi'an Research Institute of High Technology, Hongqing Town, Xi'an, in 2009 and 2014, respectively, where he is currently a Post-Doctoral Researcher. His research interests include vehicular attitude determination, land-vehicle navigation, and mobile satellite communication.